

Resource-efficient analyzer of Bell and Greenberger-Horne-Zeilinger states of multiphoton systems

Tao Li^{1,2}, Adam Miranowicz^{2,3}, Keyu Xia⁴, and Franco Nori (野理)^{2,5}

¹School of Science, Nanjing University of Science and Technology, Nanjing 210094, China

²Theoretical Quantum Physics Laboratory, RIKEN Cluster for Pioneering Research, Wako-shi, Saitama 351-0198, Japan

³Faculty of Physics, Adam Mickiewicz University, PL-61-614 Poznań, Poland

⁴College of Engineering and Applied Sciences, Nanjing University, Nanjing 210093, China

⁵Physics Department, The University of Michigan, Ann Arbor, Michigan 48109-1040, USA



(Received 5 November 2018; revised manuscript received 26 September 2019; published 1 November 2019)

We propose a resource-efficient error-rejecting entangled-state analyzer for polarization-encoded multiphoton systems. Our analyzer is based on two single-photon quantum-nondemolition detectors, where each of them is implemented with a four-level emitter (e.g., a quantum dot) coupled to a one-dimensional system (such as a micropillar cavity or a photonic nanocrystal waveguide). The analyzer works in a passive way and can completely distinguish 2^n Greenberger-Horne-Zeilinger (GHZ) states of n photons without using any active operation or fast switching. The efficiency and fidelity of the GHZ-state analysis can, in principle, be close to unity, when an ideal single-photon scattering condition is fulfilled. For a nonideal scattering, which typically reduces the fidelity of a GHZ-state analysis, we introduce a passively error-rejecting circuit to enable a near-perfect fidelity at the expense of a slight decrease of its efficiency. Furthermore, the protocol can be directly used to perform a two-photon Bell-state analysis. This passive, resource-efficient, and error-rejecting protocol can, therefore, be useful for practical quantum networks.

DOI: [10.1103/PhysRevA.100.052302](https://doi.org/10.1103/PhysRevA.100.052302)

I. INTRODUCTION

Quantum entanglement is a fascinating phenomenon in quantum physics [1], which provides a promising platform for various quantum technologies, including quantum communication networks [2]. Sharing quantum entanglement among distant network nodes is a prerequisite for many practical applications [3–9]. There are two main obstacles for practical applications of multipartite quantum entanglement, i.e., entanglement generation over desired nodes and entanglement analysis within a local node. Usually, it is difficult to distribute local entanglement over spatially separated nodes due to channel high losses [10]. An efficient method to overcome channel noise uses quantum repeaters [11–14], which are based on entanglement purification [15–18] and quantum swapping [19–23]. By applying a proper entanglement analysis and local operations, one can complete an entanglement-purification protocol to distill some entanglement of a higher fidelity, and enlarge the distance of an entangled channel through quantum swapping. In addition to entanglement purification and entanglement swapping, Bell-state analysis is crucial, e.g., for quantum teleportation [8,9], quantum secure direct communication [24–27], and quantum dense coding [28]. It plays an essential role in various entanglement-based quantum information processing protocols [7–28].

Multipartite entanglement, compared to two-particle entanglement, is more powerful to reveal the nonlocality of quantum physics [1,28–30]. The Greenberger-Horne-Zeilinger (GHZ) states enable more refined demonstrations of quantum nonlocality, and can be used to build more complex quantum networks involving many nodes [31–34] and to

perform, i.e., conference-key agreement [35]. Furthermore, GHZ states enable efficient methods for large-scale cluster-state generation for measurement-based quantum computing [36–42], and also provide a useful basis for quantum metrology [43,44]. The generation and analysis of n -photon GHZ entanglement are highly demanding. To date, various efficient methods to generate the GHZ entanglement have been developed for different physical systems [45–53]. In photonic systems, an eight-photon GHZ state and a three-photon high-dimensional GHZ state have been experimentally demonstrated [54–57] by performing quantum fusion combined with post-selection operations and quantum interference [28,58,59]. By using a time delay, a resource-efficient method was proposed and demonstrated [60] for generating a six-photon GHZ state.

It is possible to generate photonic GHZ states or other multipartite-entangled states in a deterministic way based on nonlinear processes [61–65]. However, it is difficult to distribute such a GHZ state efficiently to distant nodes, due to the inefficiency of the GHZ sources and high losses during transmission [10,66]. One possible solution is to establish entanglement pairs between a center node and distant nodes in parallel [11–14], and then to perform quantum swapping together with a GHZ-state analysis in the center node [67,68].

In 1998, Pan and Zeilinger proposed, to our knowledge, the first practical GHZ-state analysis with linear-optical elements [69]. Their proposal can identify two of n -photon GHZ states by post-selection operations. In principle, one can constitute a nearly deterministic n -photon GHZ-state analysis with linear optics, when massive ancillary photons are used [70]. However, according to the Cansamiglia-

Lütkenhaus no-go theorem [71], perfect and deterministic Bell-state analysis on two polarization-encoded qubits is impossible by using only linear-optical elements (in addition to photodetectors) and auxiliary modes in the vacuum state. By taking into account nonlinear processes, a complete GHZ-state analysis for photonic systems becomes possible [72,73], and can achieve perfect efficiency and fidelity for an ideal process. Moreover, a complete entangled-state analysis for hyperentangled or redundantly encoded photon pairs is possible [74–79]. The existing GHZ-state analyses typically require active operations and/or fast switching, and always require more quantum resources when the photon number of a given GHZ state increases. Furthermore, the fidelity of the Bell-state or GHZ-state analyses significantly depends on the nonlinearity strength of realistic nonlinear processes [65]. A deviation from an ideal nonlinear process leads to errors and, thus, reduces the fidelity. These disadvantages significantly limit applications of a GHZ-state analysis for practical quantum networks.

Here we propose a resource-efficient passive protocol of a multiphoton GHZ-state analysis using only two single-photon nondestructive [quantum nondemolition (QND)] detectors, three standard (destructive) single-photon detectors, and some linear-optical elements. The GHZ-state analysis circuit is universal, and can completely distinguish 2^n GHZ states with different photon numbers n , according to the measurement results of single-photon nondestructive and destructive detectors. The circuit works in a passive way as the Pan-Zeilinger GHZ-state analyzer does [69]. During the entangled-state analysis, there are neither active operations on ancillary atoms nor adaptive switching of photons [80]. The efficiency of our GHZ-state analysis can, in principle, be equal to one. Moreover, our protocol has no requisite for direct Hong-Ou-Mandel interference which requires simultaneous operations on two individual photons. Thus, we can significantly simplify the process of GHZ-state analysis and, subsequently, the structure of multinode quantum networks. Furthermore, the detrimental effect on the fidelity, introduced by a nonideal scattering process, can be eliminated passively at the expense of a decrease of its efficiency. Therefore, our protocol is resource efficient and passive, and can be used to efficiently entangle distant nodes in complex quantum networks.

The paper is organized as follows: A quantum interface between a single photon and a single quantum dot (QD) is introduced briefly in Sec. II for performing QND measurements on linearly polarized photons. In Sec. III, a passive GHZ-state analysis circuit is presented. In Sec. IV, a method to efficiently generate entanglement among distant nodes is described. Subsequently, the performance of the circuit, with state-of-the-art experimental parameters, is discussed in Sec. V. We conclude with brief discussion and conclusions in Secs. VI and VII. Moreover, Appendixes A and B present the two simplest examples of our method for the analysis of two-photon Bell states and three-photon GHZ states.

II. SINGLE-PHOTON QND DETECTOR

An efficient interface, between a single photon and a single emitter, constitutes a necessary building block for various kinds of quantum tasks, especially for long-distance or dis-

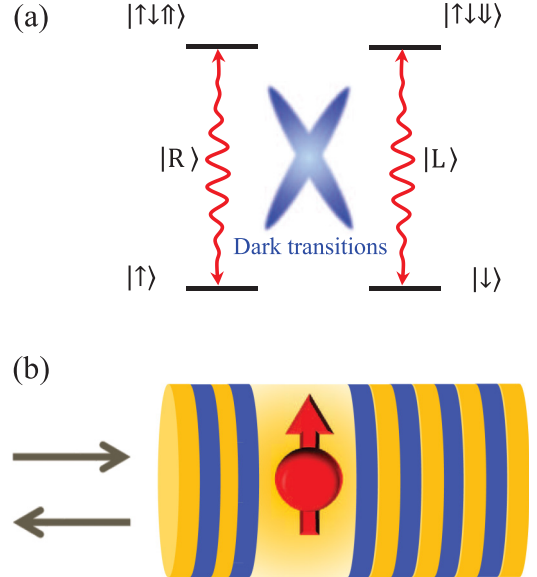


FIG. 1. Proposal of quantum-nondemolition detection based on spin-dependent transitions for the negatively charged exciton X^- . (a) Relative-level structure and optical transition of a singly charged quantum dot (QD); (b) a QD coupled to an optical micropillar cavity. Here, $|\uparrow\rangle$ ($|\downarrow\rangle$) denotes the electron spin state with J_z equal to $1/2$ ($-1/2$), and $|\uparrow\downarrow\uparrow\rangle$ ($|\uparrow\downarrow\downarrow\rangle$) denotes the trion state of X^- with J_z equal to $3/2$ ($-3/2$). A photon in a right- (left-) circularly polarized state $|R\rangle$ ($|L\rangle$) can only couple to the transition $|\uparrow\rangle \leftrightarrow |\uparrow\downarrow\uparrow\rangle$ ($|\downarrow\rangle \leftrightarrow |\uparrow\downarrow\downarrow\rangle$). Therefore, the cross transitions are forbidden by the quantum-optical selection rules.

tributed quantum networks [2,65]. To begin with, we consider a process of single-photon scattering by a four-level emitter coupled to a one-dimensional system, such as a QD coupled to a micropillar cavity or a photonic nanocrystal waveguide [81–86]. A singly charged self-assembled In(Ga)As QD has four energy levels [85–87]: two ground states of $J_z = \pm 1/2$, denoted as $|\uparrow\rangle$ and $|\downarrow\rangle$, respectively; and two optically excited trion states X^- , consisting of two electrons and one hole, with $J_z = \pm 3/2$, denoted as $|\uparrow\downarrow\uparrow\rangle$ and $|\uparrow\downarrow\downarrow\rangle$, respectively. Here the quantization axis z is along the growth direction of the QD and it is the same as the direction of the input photon. Therefore, there are two circularly polarized dipole transmissions which are degenerated when the environment magnetic field is zero, as shown in Fig. 1. A right-circularly polarized photon $|R\rangle$ and a left-circularly polarized photon $|L\rangle$ can only couple to the transitions $|\uparrow\rangle \leftrightarrow |\uparrow\downarrow\uparrow\rangle$ and $|\downarrow\rangle \leftrightarrow |\uparrow\downarrow\downarrow\rangle$, respectively.

The single-photon scattering process of a QD-cavity unit is dependent on the state of the QD. There are two individual cases: (1) If an input photon does not match the circularly polarized transition of the QD, the photon excites the cavity mode that is orthogonal to the polarization transition of the QD, and it is reflected by a practically empty cavity with a loss probability caused by photon absorption and/or side leakage. (Hereafter, for brevity, we refer to the side leakage only, but we also mean other photon absorption losses.) However, (2) if an input photon matches a given transition of the QD, the photon interacts with the QD and is reflected by the cavity that couples to the QD. Therefore, a j -circularly polarized photon

(where $j = \text{right or left}$) in the input mode $\hat{a}_{\omega_j, \text{in}}^\dagger$ of frequency ω_j , after it is scattered by a QD-cavity unit, evolves into an output mode $\hat{a}_{\omega_j, \text{out}}^\dagger$ as follows [84–87]:

$$\begin{aligned}\hat{a}_{\omega_j, \text{in}}^\dagger |0, 0, \bar{s}\rangle &\rightarrow r_0 \hat{a}_{\omega_j, \text{out}}^\dagger |0, 0, \bar{s}\rangle, \\ \hat{a}_{\omega_j, \text{in}}^\dagger |0, 0, s\rangle &\rightarrow r_1 \hat{a}_{\omega_j, \text{out}}^\dagger |0, 0, s\rangle,\end{aligned}\quad (1)$$

where the state $|0, 0, s\rangle$ ($|0, 0, \bar{s}\rangle$) denotes that both input and output fields are in the vacuum state and the QD is in the state $|s\rangle$ ($|\bar{s}\rangle$) that couples (does not couple) to the input photon. Under the assumptions of both adiabatic evolution of the cavity field and negligible excitation of the QD, the state-dependent reflection amplitudes r_0 and r_1 , corresponding, respectively, to the aforementioned cases (1) and (2), are given by [84–87]

$$\begin{aligned}r_0(\omega) &= 1 - \frac{\kappa}{i(\omega_c - \omega) + \frac{\kappa}{2} + \frac{\kappa_s}{2}}, \\ r_1(\omega) &= 1 - \frac{\kappa f}{[i(\omega_c - \omega) + \frac{\kappa}{2} + \frac{\kappa_s}{2}]f + g^2},\end{aligned}\quad (2)$$

where the auxiliary function f is given by $f = i(\omega_{X-} - \omega) + \frac{\gamma}{2}$. Here ω_{X-} is the transmission frequency of the QD and ω_c is the resonant frequency of the cavity. These frequencies can be tuned to be equal to $\omega_{X-} = \omega_c$, for simplicity. Moreover, κ describes a directional coupling between the cavity modes and the input and output modes; g denotes the coupling between the QD and cavity; κ_s represents the cavity side-leakage rate, and γ is the trion decay rate. These formulas for the reflection coefficients are valid in general for both weak and strong couplings [88].

For ideal scattering in the strong-coupling regime with $\kappa_s \ll \kappa$ and $\gamma, \kappa \ll g$ (or in the high-cooperativity regime with $\kappa_s \ll \kappa$, $\gamma \ll g \ll \kappa$, and $\gamma\kappa \ll g^2$) [88], an input photon, that is resonant with a QD transition, is deterministically reflected by the QD-cavity unit. A π -phase (*zero*-phase) shift is introduced to the hybrid system consisting of a photon and the QD with $r_0 = -1$ for $g = 0$ ($r_1 = 1$ for $\kappa\gamma \ll g^2$), if the photon decouples (couples) to a transition of the QD. When the QD is initialized to be in the superposition state $|\pm\rangle = (|\uparrow\rangle \pm |\downarrow\rangle)/\sqrt{2}$, an input photon in a linearly polarized state evolves as follows:

$$\begin{aligned}|H\rangle |\pm\rangle &\rightarrow |V\rangle |\mp\rangle, \\ |V\rangle |\pm\rangle &\rightarrow |H\rangle |\mp\rangle.\end{aligned}\quad (3)$$

Equation (3) means that if a QD receives a single photon, then it receives the Pauli σ_x unitary. On the one hand, if the QD does not receive any photon, then it does not change its state. Thus, if we can identify whether the QD receives the Pauli σ_x unitary, then it works as a QND measurement for photons [85,88–90]. Furthermore, when the QD receives a photon, then it flips the polarization state of the photon simultaneously [91,92]. We will show in Sec. V that the QND measurement can work faithfully with a limited efficiency for practical scattering, i.e., when $r_1(\omega)$ and $r_0(\omega)$ significantly deviate from their ideal values ± 1 .

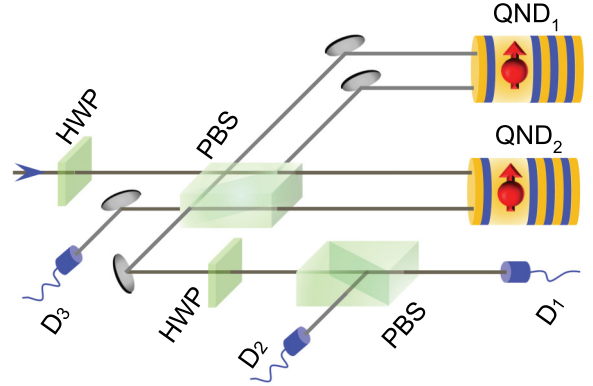


FIG. 2. Schematics of the passive optical GHZ-state analyzer using single-photon QND detectors. Here PBS denotes a polarizing beam splitter, which transmits photons with horizontal polarization $|H\rangle$ and reflects those with vertical polarization $|V\rangle$. HWP represents a half-wave plate that performs the Hadamard transformation on photons passing it, i.e., $|H\rangle \rightarrow (|H\rangle + |V\rangle)/\sqrt{2}$ or $|V\rangle \rightarrow (|H\rangle - |V\rangle)/\sqrt{2}$. QND detection completes a nondestructive measurement on single photons, and D_i ($i = 1, 2, 3$) is an ordinary (destructive) single-photon detector.

III. PASSIVE GHZ-STATE ANALYZER

A. The setup

So far, we have described a QND detection of linearly polarized single photons. In this section, we describe how to incorporate a QND detector into the setup for the passive optical GHZ-state analysis, as shown in Fig. 2. The setup is composed of two half-wave plates (HWPs), two polarizing beam splitters (PBSs), two single-photon QND detectors in the state $|+\rangle_1 |+\rangle_2$, and several standard (destructive) single-photon detectors. The HWP is tuned to perform the Hadamard transformation on photons passing it, i.e., $|H\rangle \rightarrow (|H\rangle + |V\rangle)/\sqrt{2}$ or $|V\rangle \rightarrow (|H\rangle - |V\rangle)/\sqrt{2}$. The PBS transmits linearly polarized photons in the state $|H\rangle$ and reflects photons in the state $|V\rangle$. The single-photon QND and standard detectors complete the photon on-off measurements in nondestructive and destructive ways, respectively.

B. GHZ states

For n -photon polarization-encoded GHZ states, the simplest two can be expressed as [28]

$$\begin{aligned}|\text{GHZ}_{00\dots 0}\rangle &= \frac{1}{\sqrt{2}}(|H\rangle^{\otimes n} + |V\rangle^{\otimes n}), \\ |\text{GHZ}_{00\dots 1}\rangle &= \frac{1}{\sqrt{2}}(|H\rangle^{\otimes n} - |V\rangle^{\otimes n}),\end{aligned}\quad (4)$$

where the last (n th) bit in the subscript of $|\text{GHZ}_{00\dots n}\rangle$ refers to the phase (\pm). If a photon is determined in the state $|H\rangle$ or $|V\rangle$, the remaining $(n-1)$ photons collapse into the same polarization. To constitute a complete basis for the n -photon system, one should take the remaining $(2^n - 2)$ orthogonal

basis states into consideration,

$$\begin{aligned} |\text{GHZ}_{i_1 i_2 \dots i_n}\rangle &= \bigotimes_{j=1}^{n-1} \sigma_{x_j}^{i_j} \otimes \sigma_{z_n}^{i_n} |\text{GHZ}_{00\dots 0}\rangle \\ &= i\sigma_{y_n}^{i_n} \bigotimes_{j=1}^n \sigma_{x_j}^{i_j} |\text{GHZ}_{00\dots 0}\rangle, \end{aligned} \quad (5)$$

which can be generated from $|\text{GHZ}_{00\dots 0}\rangle$ by performing a single-photon rotation on each photon, and

$$\bigotimes_{j=1}^n \sigma_{x_j}^{i_j} = \sigma_{x_1}^{i_1} \otimes \sigma_{x_2}^{i_2} \otimes \dots \otimes \sigma_{x_n}^{i_n}.$$

Here, the superscripts $i_1, i_2, \dots, i_n \in \{0, 1\}$, the Pauli operators $\sigma_{x_j} = |H\rangle_j \langle V| + |V\rangle_j \langle H|$ perform a polarization flip on the j th photon with $j = 1, 2, \dots, n$; $\sigma_{y_n} = -i(|H\rangle_n \langle V| - |V\rangle_n \langle H|)$; $\sigma_{z_n} = |H\rangle_n \langle H| - |V\rangle_n \langle V|$ performs a phase flip on the n th photon; and the relative phase between the two components of Eq. (5) is determined by i_n ; i.e., $i_n = 0$ ($i_n = 1$) leads to a relative phase of 0 (π).

C. State transformations for the GHZ-state analysis

Now we focus on completely distinguishing the aforementioned 2^n GHZ states, which is of vital importance for multiuser quantum networks [67–69]. According to stabilizer theory [93–96], the n -photon state $|\text{GHZ}_{00\dots 0}\rangle$, given in Eq. (4), is a stabilizer state that can be uniquely defined by n stabilizing operators S_k ,

$$S_k = \begin{cases} \sigma_{x_1} \otimes \sigma_{x_2} \otimes \dots \otimes \sigma_{x_n}, & k = 1; \\ \sigma_{z_{k-1}} \otimes \sigma_{z_k}, & k = 2, 3, \dots, n. \end{cases} \quad (6)$$

Here the operators σ_{z_k} perform a phase flip on the k th photon with $k = 1, 2, \dots, n$; there is an implicit identity $I^{\otimes(n-2)}$ acting on the remaining photons that is suppressed in $S_{k \geq 2}$ for simplicity.

The set of operators S_1, S_2, \dots, S_n forms a complete set of commuting observables; the 2^n GHZ states are common eigenvectors of all S_k 's with different eigenvalues [94], i.e., $|\text{GHZ}_{00\dots 0}\rangle$ gives an eigenvalue +1 for all S_k 's. Therefore, we can measure the stabilizing operators S_k 's to completely discriminate 2^n GHZ states of an n -photon system.

Here the n -photon observable S_1 corresponds to the measurement of the relative phase between the two terms in a GHZ state and can be nondestructively measured by using two QND detectors introduced in Sec. II; $S_{k \geq 2}$ corresponds to parity detection on the pair of $(k-1)$ th and k th photons and is measured with direct polarization measurements on each photon scattered by the QND detectors. To explain in detail our GHZ-state analysis, we use the ket notation instead of the stabilizer codes, since the stabilizer states change during the analysis.

For clarity, we divide this GHZ-state analysis into several steps. Let us suppose that there is a spatial separation between each two optical elements such that all photons can pass a given optical element before entering another element. Note this requirement is not necessary, and we will demonstrate, in the next section, that our proposal also works when each

photon is passing one by one from the input port to the output port and is measured by a single-photon destructive detector.

After passing n photons through the HWP, the Hadamard transformation is performed on each photon, and the 2^n GHZ states are changed into superposition states of 2^{n-1} (out of 2^n possible) product states, each with an even (odd) number of V -polarized photons for $|\text{GHZ}_{i_1 i_2 \dots i_{n-1} 0}\rangle$ ($|\text{GHZ}_{i_1 i_2 \dots i_{n-1} 1}\rangle$). For instance, the states $|\text{GHZ}_{i_1 i_2 \dots i_{n-1} 0}\rangle$ and $|\text{GHZ}_{i_1 i_2 \dots i_{n-1} 1}\rangle$, after the Hadamard transformation of each photon, evolve into

$$\begin{aligned} |\Psi_1\rangle &= \frac{1}{\sqrt{2^{n-1}}} \sum_{m=0}^{\lfloor \frac{n}{2} \rfloor} \sqrt{C_n^m} |G_{2m}^{i_1, \dots, i_{n-1}}\rangle, \\ |\Phi_1\rangle &= \frac{1}{\sqrt{2^{n-1}}} \sum_{m=1}^{\lfloor \frac{n+1}{2} \rfloor} \sqrt{C_n^{m-1}} |G_{2m-1}^{i_1, \dots, i_{n-1}}\rangle, \end{aligned} \quad (7)$$

respectively. Here $[x]$ is the integer value function that rounds the number x down to the nearest integer; $C_n^m = \frac{n!}{m!(n-m)!}$ is the binomial coefficient; the state $|G_m^{i_1, \dots, i_{n-1}}\rangle$ is an n -photon superposition state that contains m V -polarized photons and $(n-m)$ H -polarized photons as follows:

$$|G_m^{i_1, \dots, i_{n-1}}\rangle = \frac{Z}{\sqrt{C_n^m}} \sum_{l_1, \dots, l_n \in \{0, 1\}} \delta_{m, m'} \bigotimes_{j=1}^n \sigma_{x_j}^{l_j} |H\rangle^{\otimes n}, \quad (8)$$

where $m' = \sum_{j=1}^n l_j$ and $\delta_{m, m'}$ is the Kronecker delta. The phase of each component is determined by the operator $Z = \bigotimes_{j=1}^{n-1} \sigma_{z_j}^{i_j}$, which is simplified to an identity operator when analyzing $|\text{GHZ}_{00\dots 0}\rangle$ and $|\text{GHZ}_{00\dots 1}\rangle$.

D. Measurements for the GHZ-state analysis

As follows from the above analysis, the relative phase of $|\text{GHZ}_{i_1 i_2 \dots i_n}\rangle$, which is determined by i_n , can be read out by measuring the number of V -polarized photons in the even-odd basis after applying the Hadamard transformation to $|\text{GHZ}_{i_1 i_2 \dots i_n}\rangle$. This measurement can be completed by a setup consisting of a PBS and two QD-cavity units (referred to as QND detectors). As demonstrated in Sec. II, a linearly polarized photon, after being scattered by a QND detector, changes its polarization state into an orthogonal state and flips the state of the detector QD. After all photons are either transmitted or reflected by the first PBS, and scattered by the QND detectors, the hybrid states of the two QDs and the n photons, corresponding to the states $|\text{GHZ}_{i_1 i_2 \dots i_{n-1} 0}\rangle$ and $|\text{GHZ}_{i_1 i_2 \dots i_{n-1} 1}\rangle$, evolve, respectively, into

$$\begin{aligned} |\Psi_2^e\rangle &= \bigotimes_{j=1}^n \sigma_{x_j} |\Psi_1\rangle |+\rangle_1 |+\rangle_2, \\ |\Phi_2^e\rangle &= \bigotimes_{j=1}^n \sigma_{x_j} |\Phi_1\rangle |-\rangle_1 |-\rangle_2, \end{aligned} \quad (9)$$

if n is even, and into

$$\begin{aligned} |\Psi_2^e\rangle &= \bigotimes_{j=1}^n \sigma_{x_j} |\Psi_1\rangle |+\rangle_1 |-\rangle_2, \\ |\Phi_2^o\rangle &= \bigotimes_{j=1}^n \sigma_{x_j} |\Phi_1\rangle |-\rangle_1 |+\rangle_2, \end{aligned} \quad (10)$$

if n is odd. The combined states of the two QDs in QND detectors are different, and can be used to deterministically distinguish $|\Psi_1\rangle$ from $|\Phi_1\rangle$ for both cases of even and odd n .

To make this point clearer, we continue our analysis to measure the parity of each photon pair $[k-1, k]$ for the case of an arbitrary *even* n . Now, photons in different polarization states combine again at the first PBS, which is followed by an HWP. The HWP completes the Hadamard transformation on each photon passing through it and evolves the photonic component of the hybrid states into its original GHZ state, up to a phase difference π . For the states $|\Psi_2^e\rangle$ and $|\Phi_2^o\rangle$, given in Eq. (9), they evolve into

$$\begin{aligned} |\Psi_3\rangle &= \pm |\text{GHZ}_{i_1 i_2 \dots i_{n-1} 0}\rangle |+\rangle_1 |+\rangle_2, \\ |\Phi_3\rangle &= \pm |\text{GHZ}_{i_1 i_2 \dots i_{n-1} 1}\rangle |-\rangle_1 |-\rangle_2. \end{aligned} \quad (11)$$

Here $|\text{GHZ}_{i_1 i_2 \dots i_{n-1} 0}\rangle$ and $|\text{GHZ}_{i_1 i_2 \dots i_{n-1} 1}\rangle$ are the n -photon GHZ states given in Eq. (5); their sign is determined by the summation of the first $(n-1)$ subscripts with $m'' = \sum_{j=1}^{n-1} i_j$, i.e., “+” for even m'' and “-” for odd m'' . Subsequently, a photon-polarization measurement setup, consisting of a PBS and two destructive single-photon detectors D_1 and D_2 , is used to detect the polarization of each photon and then divides the measurement results according to the number of clicks of each detector, i.e., when n H -polarized (V -polarized) photons are detected, the n input photons are projected into either $|\text{GHZ}_{00\dots 0}\rangle$ or $|\text{GHZ}_{00\dots 1}\rangle$, which can be distinguished by detecting the state of the QD in each QND detector.

It is seen that there is neither active feedback nor fast switching operations involved in the entangled-state analysis. The setup works in a completely passive way, which is similar to that based on linear-optical elements and single-photon detectors. When $n = 2$, the GHZ-state analysis setup enables a passive Bell-state analysis for two-photon systems, which are typically denoted as

$$\begin{aligned} |\phi^\pm\rangle &= \frac{1}{\sqrt{2}}(|H\rangle|H\rangle \pm |V\rangle|V\rangle), \\ |\psi^\pm\rangle &= \frac{1}{\sqrt{2}}(|H\rangle|V\rangle \pm |V\rangle|H\rangle). \end{aligned} \quad (12)$$

Detailed analyses for $n = 2$ and 3 are presented in Appendixes A and B, respectively.

IV. EFFICIENT DISTANT MULTIPARTITE ENTANGLEMENT GENERATION FOR QUANTUM NETWORKS

In quantum multinode networks, multipartite entanglement among many nodes is useful for practical quantum communication or distributed quantum computation [28,29]. A direct method for sharing the GHZ entanglement among several distant nodes can be enabled by a faithful entanglement

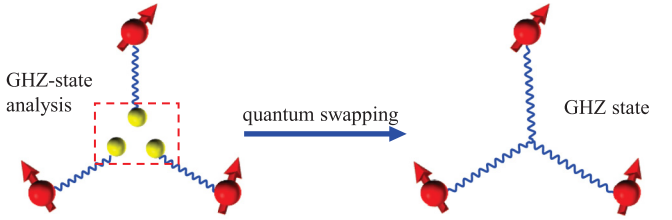


FIG. 3. Schematics of nonlocal GHZ-state generation for multi-party quantum networks. Here a red circle with an arrow represents a stationary qubit, while a yellow circle represents a photon. Each wave line represents entanglement between the particles it connects.

distribution after locally generating the GHZ entanglement. However, the efficiency of such a multipartite entanglement distribution significantly decreases with the increasing photon number involved in the GHZ entanglement [10]. Furthermore, the experimental methods for generating multiphoton GHZ entanglement are still inefficient due to the limited experimental technologies. A significantly more efficient method for distant GHZ-state generation can be achieved by entanglement swapping. In the following, we describe a scheme for the GHZ entanglement generation among three stationary qubits, and these stationary qubits can be atomic ensembles, nitrogen-vacancy (NV) centers, QDs, and other systems [97].

Suppose there are three communicating nodes in a quantum network, say, Alice, Bob, and Charlie. An ancillary node (Eve) shares hybrid entanglement pairs with Alice, Bob, and Charlie, respectively, as follows [11–18]:

$$|\phi\rangle_{ji} = \frac{1}{\sqrt{2}}(|\uparrow\rangle_j|H\rangle_i + |\downarrow\rangle_j|V\rangle_i), \quad (13)$$

where the subscript i (with $i = a, b, c$) represents the photons owned by Eve, and it is entangled with the j th QD (with $j = A, B, C$), which belongs to Alice, Bob, and Charlie, respectively, as shown in Fig. 3. The state $|\phi\rangle_{Aa}|\phi\rangle_{Bb}|\phi\rangle_{Cc}$ of the three hybrid entanglement pairs Aa , Bb , and Cc can be rewritten as

$$|\phi_0\rangle = \frac{1}{2\sqrt{2}} \sum_{i,j,k} |\text{GHZ}_{ijk}\rangle_{ABC} |\text{GHZ}_{ijk}\rangle_{abc}. \quad (14)$$

Here the subscripts $i, j, k \in \{0, 1\}$, and the polarization-encoded GHZ states $|\text{GHZ}_{ijk}\rangle_{abc}$ are defined in Eq. (5) for $n = 3$. The eight distant stationary GHZ states among Alice, Bob, and Charlie are of the following forms:

$$\begin{aligned} |\text{GHZ}_{00k}\rangle_{ABC} &= \frac{1}{\sqrt{2}}[|\uparrow\rangle_A|\uparrow\rangle_B|\uparrow\rangle_C + (-1)^k|\downarrow\rangle_A|\downarrow\rangle_B|\downarrow\rangle_C], \\ |\text{GHZ}_{10k}\rangle_{ABC} &= \frac{1}{\sqrt{2}}[|\downarrow\rangle_A|\uparrow\rangle_B|\uparrow\rangle_C + (-1)^k|\uparrow\rangle_A|\downarrow\rangle_B|\downarrow\rangle_C], \\ |\text{GHZ}_{01k}\rangle_{ABC} &= \frac{1}{\sqrt{2}}[|\uparrow\rangle_A|\downarrow\rangle_B|\uparrow\rangle_C + (-1)^k|\downarrow\rangle_A|\uparrow\rangle_B|\downarrow\rangle_C], \\ |\text{GHZ}_{11k}\rangle_{ABC} &= \frac{1}{\sqrt{2}}[|\downarrow\rangle_A|\downarrow\rangle_B|\uparrow\rangle_C + (-1)^k|\uparrow\rangle_A|\uparrow\rangle_B|\downarrow\rangle_C], \end{aligned} \quad (15)$$

with $k \in \{0, 1\}$. These states constitute a complete basis for three-QD systems.

When the ancillary node Eve performs a quantum swapping operation with a three-photon polarization-encoded GHZ-state analysis, the states of the three stationary qubits, which belong to Alice, Bob, and Charlie, are projected into a deterministic GHZ state according to the analysis result of Eve. That is, we can, in principle, generate multipartite GHZ entanglement efficiently among distant stationary qubits with a perfect efficiency.

In Sec. III, we have described a particular pattern of the GHZ-state analysis with a preset time delay between each two optical elements. Now we demonstrate that the GHZ-state analysis also works for a time-delay free pattern, by performing the aforementioned quantum swapping as an example. Suppose both QDs in the QND detectors are initialized in the state $|+\rangle = (| \uparrow \rangle + | \downarrow \rangle)/\sqrt{2}$, and all the linear-optical elements perform the same operation as that described in Sec. III. The three photons from hybrid entanglement pairs Aa , Bb , and Cc , subsequently pass through the analysis setup independently, rather than transmitting them in a block pattern. After photon a passing through the setup and being routed into two spatial modes that are ended with single-photon detectors, the hybrid system, consisting of three entanglement pairs and two QDs in the QND detectors, evolves into

$$\begin{aligned} |\phi_1\rangle = \frac{1}{2} & [|H\rangle_a(|+\rangle_A|+\rangle_1|-\rangle_2 + |-\rangle_A|-\rangle_1|+\rangle_2) \\ & - |V\rangle_a(|+\rangle_A|+\rangle_1|-\rangle_2 - |-\rangle_A|-\rangle_1|+\rangle_2] \otimes |\phi\rangle_{Bb}|\phi\rangle_{Cc}. \end{aligned} \quad (16)$$

For clarity, we assume that the standard (destructive) single-photon detectors work nondestructively and a photon survives after a measurement on it, such that we can directly specify the state of the distant stationary qubits according to the state of the photon a . Subsequently, the photon b is input into the setup when the photon a has passed through the setup and lead to a click of either single-photon destructive detector D_1 or D_2 . The hybrid system evolves into

$$\begin{aligned} |\phi_2\rangle = \frac{1}{2\sqrt{2}} & [(|\Phi^+\rangle_{AB}|+\rangle_1|+\rangle_2 \\ & + |\Phi^-\rangle_{AB}|-\rangle_1|-\rangle_2)|H\rangle_a|H\rangle_b - (|\Psi^+\rangle_{AB}|+\rangle_1|+\rangle_2 \\ & + |\Psi^-\rangle_{AB}|-\rangle_1|-\rangle_2)|H\rangle_a|V\rangle_b - (|\Psi^+\rangle_{AB}|+\rangle_1|+\rangle_2 \\ & - |\Psi^-\rangle_{AB}|-\rangle_1|-\rangle_2)|V\rangle_a|H\rangle_b + (|\Phi^+\rangle_{AB}|+\rangle_1|+\rangle_2 \\ & - |\Phi^-\rangle_{AB}|-\rangle_1|-\rangle_2)|V\rangle_a|V\rangle_b] \otimes |\phi\rangle_{Cc}, \end{aligned} \quad (17)$$

where the four Bell states of the two QDs, belonging to Alice and Bob, are as follows:

$$\begin{aligned} |\Phi^\pm\rangle_{AB} &= \frac{1}{\sqrt{2}}(|\uparrow\rangle_A|\uparrow\rangle_B \pm |\downarrow\rangle_A|\downarrow\rangle_B), \\ |\Psi^\pm\rangle_{AB} &= \frac{1}{\sqrt{2}}(|\uparrow\rangle_A|\downarrow\rangle_B \pm |\downarrow\rangle_A|\uparrow\rangle_B). \end{aligned} \quad (18)$$

Now, if Eve terminates the input of photon c and detects the two QDs of the QND detectors, the two distant QDs A and B are collapsed to one of the Bell states given in Eq. (18), according to the results of the QND detectors and the measurement on photons ab . That is, a deterministic quantum swapping operation can be completed between two

hybrid entanglement pairs Aa and Bb by using the passive entanglement analysis setup.

If Eve inputs the photon c into the analysis setup rather than terminating it with a measurement on the two QDs of the QND detectors, the state $|\phi_2\rangle$ of the hybrid system evolves into the final state,

$$\begin{aligned} |\phi_3\rangle = \frac{1}{2\sqrt{2}} \sum_{ij} (-1)^{i+j} & [|\text{GHZ}_{ij0}\rangle_{ABC}|\text{GHZ}_{ij1}\rangle_{abc}|+\rangle_1|-\rangle_2 \\ & + |\text{GHZ}_{ij1}\rangle_{ABC}|\text{GHZ}_{ij0}\rangle_{abc}|-\rangle_1|+\rangle_2], \end{aligned} \quad (19)$$

with the subscripts $i, j \in \{0, 1\}$. Three distant QDs A , B , and C are projected into a predetermined GHZ state, according to the results of the QND detectors and the single-photon destructive detectors, when Eve applies a polarization-encoded GHZ-state analysis on three photons of the hybrid entangled pairs. Therefore, in principle, the passive GHZ-state analysis works faithfully for both cases, i.e., the time-delay and time-delay-free cases, when an ideal single-photon QND detector is available.

V. PERFORMANCE OF THE PASSIVE GHZ-STATE ANALYZER

A. Realistic photon scattering

A core element of the passive GHZ-state analysis is the QND detector for single photons. Here a unit consisting of a QD and a micropillar cavity enables such QND detection. In principle, the QND detector can perfectly distinguish two orthogonal polarization states $|H\rangle$ and $|V\rangle$ of a single photon with perfect efficiency. However, there are always some imperfections that introduce a deviation from ideal single-photon scattering [82–86], such as a finite single-photon bandwidth, a finite coupling g between a QD and a cavity, and the nondirectional cavity side leakage κ_s , etc. This leads to realistic (nonideal) scattering for a linearly polarized photon. Thus, the hybrid system consisting of a linearly polarized single photon and a QD, evolves as follows:

$$\begin{aligned} |H\rangle|\pm\rangle &\rightarrow \frac{1}{\sqrt{C_N}}[(r_1 + r_0)|H\rangle|\pm\rangle + (r_1 - r_0)|V\rangle|\mp\rangle], \\ |V\rangle|\pm\rangle &\rightarrow \frac{1}{\sqrt{C_N}}[(r_1 - r_0)|H\rangle|\mp\rangle + (r_1 + r_0)|V\rangle|\pm\rangle], \end{aligned} \quad (20)$$

where the parameters r and r_0 are frequency-dependent reflection coefficients given in Eq. (2); $C_N = 2(|r_1|^2 + |r_0|^2)$ is the normalized coefficient. After scattering, the state of the photon and the QD evolves in two ways independent of its initial state.

(1) It is flipped simultaneously with a probability $p_1 = |r_1 - r_0|^2/4$, which is the desired output and it can be simplified to perform an ideal QND detection, as given in Eq. (3), when ideal scattering with $r_1 = 1$ and $r_0 = -1$ is achieved.

(2) The state of the photon and the QD are unchanged with the probability $p_2 = |r_1 + r_0|^2/4$, which leads to errors and results in an unfaithful QND detection for single photons.

Fortunately, this nonideal scattering does not affect the fidelity of the passive GHZ-state analysis, since the undesired scattering component is filtered out automatically by the PBS

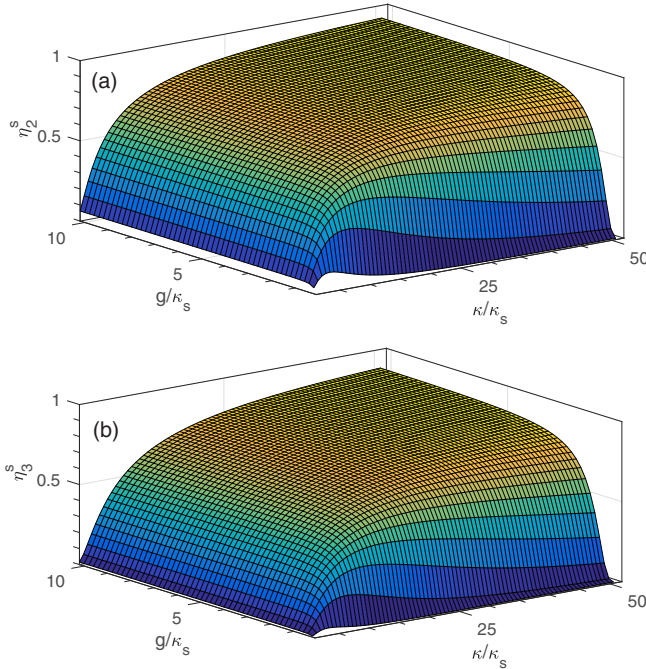


FIG. 4. Average efficiencies (a) η_2^s of the two-photon Bell-state analyzer and (b) η_3^s of the three-photon GHZ-state analyzer versus the coupling strength g/κ_s and the directional coupling rate of a cavity κ/κ_s in units of the cavity side-leakage rate κ_s . These averages are calculated over all detunings of input photons, with the Gaussian spectrum given by Eq. (23) and $\sigma_\omega = \gamma$. The decay parameters are $(\kappa_s, \gamma) = (30 \mu\text{eV}, 0.3 \mu\text{eV})$.

and only leads to an inconclusive result rather than infidelity result by a click of the single-photon destructive detector D_3 .

B. Realistic analyzer efficiency

For ideal scattering, the analyzer efficiency approaches unity. Here, we evaluate the performance of a realistic analyzer for the general reflection amplitudes given in Eq. (2). Nonideal scattering in practical QND detection does not reduce the fidelity of an n -photon GHZ analysis. However, this realistic scattering decreases the efficiency $\tilde{\eta}_n^s$, which is defined as the probability that all photons are detected by a single-photon destructive detector, either D_1 or D_2 . For monochromatic photons of a frequency ω , the efficiency $\tilde{\eta}_n^s$ is defined as

$$\tilde{\eta}_n^s = \eta_0^n \eta_1^n(\omega), \quad (21)$$

where η_0 is the efficiency of a single-photon detector D_i and $\eta_1(\omega)$ is the error-free efficiency of a practical scattering with

$$\eta_1(\omega) = \left| \frac{r_1(\omega) - r_0(\omega)}{2} \right|^2. \quad (22)$$

The average efficiencies of the passive two-photon Bell-state and the three-photon GHZ-state analyzers are shown in Fig. 4 with decay parameters $(\kappa_s, \gamma) = (30 \mu\text{eV}, 0.3 \mu\text{eV})$, which are adopted according to the QDs that are embedded in electrically controlled cavities around 4 K [98,99]. We plotted the average efficiencies η_2^s and η_3^s versus the coupling strength g/κ_s and the directional coupling rate of the cavity κ/κ_s for a

given Gaussian single-photon pulse defined by the spectrum,

$$f(\omega) = \frac{1}{\sqrt{\pi} \sigma_\omega} \exp \left[-\left(\frac{\omega - \omega_c}{\sigma_\omega} \right)^2 \right], \quad (23)$$

where ω_c is the center frequency and σ_ω denotes the pulse bandwidth with $\omega_c = \omega_{X^-}$ and $\sigma_\omega = \gamma$. Here the average efficiencies are calculated in the frequency domain. The reflection coefficients appear as a frequency-dependent redistribution function that is proportional to $|r_1(\omega) - r_0(\omega)|^{2n}$ as follows [100,101]:

$$\eta_n^s = \int d\omega f(\omega) \eta_0^n \left| \frac{r_1(\omega) - r_0(\omega)}{2} \right|^{2n}. \quad (24)$$

In general, the average efficiencies of the passive two-photon Bell-state and three-photon GHZ-state analyzers increase when the coupling g/κ_s between a QD and a cavity is increased for a given directional coupling rate κ/κ_s . This is because the cooperativity,

$$C = \frac{g^2}{\gamma \kappa_T} = \frac{g^2}{\gamma (\kappa + \kappa_s)}, \quad (25)$$

which is defined as an essential parameter quantifying the loss of an atom-cavity system, increases when we increase g/κ_s and keep other parameters unchanged. For a given g/κ_s , the average efficiencies of these two analyzers first increase and then decrease when κ/κ_s is increased, as shown in Fig. 4. This is mainly due to the competition between an increased ratio of κ/κ_s and a decreased cooperativity C . Therefore, one can maximize the efficiencies by using cavities with a mediate κ , which can be achieved, e.g., by decreasing the number of the Bragg reflector of a micropillar cavity. For simplicity, we set the efficiency of a single-photon destructive detector as $\eta_0 = 1$.

For the two-photon Bell-state analyzer, its average efficiency $\eta_2^s = 0.304$ for an experimental demonstrated coupling $g/\kappa_s = 1$ and the directional coupling rate of a cavity, $\kappa/\kappa_s = 3$, which corresponds to a cooperativity $C = 25$. For the three-photon GHZ-state analyzer, one can obtain the average efficiency $\eta_3^s \simeq 0.168$ for the same systematic parameters. If κ is increased to $\kappa/\kappa_s = 19$ with a cooperativity $C = 5$ [98], the average efficiencies are increased to $\eta_2^s \simeq 0.664$ and $\eta_3^s \simeq 0.541$, respectively. Note that the adiabatic condition is still satisfied in this case, since the photon bandwidth $\sigma_\omega = \gamma$ is much smaller than $2g^2/\kappa_T = 2C\gamma$. The protocol works with a higher efficiency for analyzing photons with a narrower bandwidth. However, this, in turn, usually increases the time period of the scattering process, and, thus, decreases the analyzer fidelity limited by QD decoherence [86,88]. The fidelity of our analyzer is given by

$$F_n(T_2) = \frac{1}{4} [1 + \exp(-t_n/T_2)]^2, \quad (26)$$

which is determined by the process for distinguishing $|\text{GHZ}_{i_1 i_2 \dots 0}\rangle$ from $|\text{GHZ}_{i'_1 i'_2 \dots 1}\rangle$ (measuring X -type stabilizer S_1), since the process for measuring Z -type stabilizers is completed directly by single-photon detectors and is independent of QD decoherence. Here, the time required to complete the n -photon GHZ-state analysis is given by $t_n \simeq n t_0$. In our numerical calculations shown in Fig. 5 and Table I, we assumed $t_0 \simeq 1.10$ ns for performing a single-photon scattering process

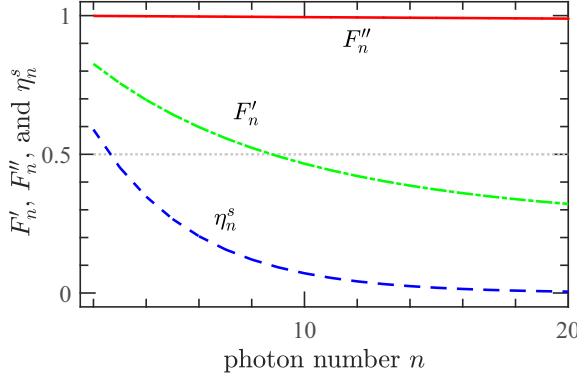


FIG. 5. Average fidelities F'_n , F''_n , and efficiency η_n^s versus photon number n . Here $F'_n \equiv F_n(T_2 = 10.9 \text{ ns})$ and $F''_n \equiv F_n(T_2 = 2 \mu\text{s})$. These averages are calculated over all detunings of input photons, with the Gaussian spectrum given by Eq. (23) and $\sigma_\omega = 2\gamma$. The decay parameters are $(\kappa_s, \gamma) = (30 \mu\text{eV}, 0.3 \mu\text{eV})$, $g = \kappa_s$, and $\kappa = 9\kappa_s$ with $C = 10$. Meanwhile, the line of the fidelities at 1/2 is shown for reference.

with a bandwidth $\sigma_\omega = 2\gamma$. Moreover, T_2 is the coherence time of the electron spin in a QD.

Typically, the coherence time T_2 is in the 1–10 ns range [87,102,103]. Taking an experimental accessible value of $T_2 = 10.9 \text{ ns}$ [102], we obtain the corresponding analyzer fidelity $F'_n \equiv F_n(T_2 = 10.9 \text{ ns})$ versus the photon number n for the parameters $(g, \kappa_s, \gamma) = (30 \mu\text{eV}, 30 \mu\text{eV}, 0.3 \mu\text{eV})$ and $\kappa/\kappa_s = 9$ with $C = 10$, as shown by the green dash-dot curve in Fig. 5 and listed Table I. For a four-photon system, the analyzer fidelity can reach $F'_4 \simeq 0.70$. For an eight-photon system, F'_8 is still larger than 0.5.

The fidelity of our GHZ-state analyzer is influenced by the coherence time T_2 . Note that the coherence time T_2 can be optimized and improved to be longer than 2 μs , when the high-degree nuclear-spin bath polarization or spin-echo refocusing methods are applied [87,103]. When $T_2 = 2 \mu\text{s}$, we can achieve the fidelity $F''_n \equiv F_n(T_2 = 2 \mu\text{s}) > 0.988$ for $n \leq 20$ (see the red solid curve in Fig. 5) assuming all the other parameters to be the same as for F'_n in this figure.

In contrast to the fidelity, the average efficiency η_n^s is independent of T_2 , because the effective output component, which is involved in a scattering process, is independent of the state of the QD, as shown in Eq. (20). In general, η_n^s decreases when the photon number n increases (see the blue dashed curve in Fig. 5 and Table I). For a 20-photon system, the average efficiency of our protocol is equal to $\eta_{20}^s = 0.0039$, which is many orders higher than the efficiency

TABLE I. Average fidelities F'_n , F''_n , and efficiency η_n^s versus photon number n for the parameters assumed in Fig. 5. Here $F'_n \equiv F_n(T_2 = 10.9 \text{ ns})$ and $F''_n \equiv F_n(T_2 = 2 \mu\text{s})$.

n	F'_n	F''_n	η_n^s	n	F'_n	F''_n	η_n^s
2	0.826	0.9989	0.5893	6	0.5981	0.9967	0.2047
3	0.7564	0.9984	0.4524	7	0.5583	0.9962	0.1572
4	0.6961	0.9978	0.3473	8	0.5235	0.9956	0.1207
5	0.6437	0.9973	0.2666	20	0.3141	0.9886	0.0039

given by $1/2^{(n-1)} = 2^{-19}$ for the standard analyzers consisting of linear-optical elements and single-photon detectors [69].

VI. DISCUSSION

The linear-optical implementation of the GHZ-state analyzer passively distinguishes two GHZ states $|\text{GHZ}_{00\dots0}\rangle$ and $|\text{GHZ}_{00\dots1}\rangle$ from the remaining $(2^n - 2)$ GHZ states, and enables a complete analysis for 2^n GHZ states when many ancillary photons and detectors are used [70]. This kind of GHZ analysis is much like a GHZ-state generation that is constructed by linear optics and post-selection [28,58,59]. Currently, the GHZ state of a 10-photon system has been demonstrated by using linear optics [104,105]. The existing GHZ-state analyzers, which are based on optical nonlinearities, have been proposed by cascading two-photon parity QND detectors [17,106]. Such an analyzer can, in principle, distinguish 2^n GHZ states of an n -photon system non-destructively, when it is assisted by fast switching and/or active operations during the entangled-state analysis. These operations dramatically increase its experimental complexity and consume more quantum resources. Furthermore, such implementations always require a strong optical nonlinearity to keep the analysis faithful.

Our scheme of a passive GHZ-state analysis for n polarization-encoded photons uses only linear-optical elements, and single-photon destructive and nondestructive detectors. This analyzer can, in principle, deterministically distinguish among 2^n GHZ states for n -photon systems, and hence it combines the advantages of those based on linear optics with those based on optical nonlinearities. Moreover, our scheme eliminates disadvantages of such standard analyzers by designing an error-tolerant QND detection for single photons, and can be useful for efficient implementations of all-photonic quantum repeaters, even including those without quantum memory [107,108].

The proposed QND detector consists of a four-level emitter coupled to a microcavity or waveguide [81–86], such as a negatively charged QD coupled to a micropillar cavity. This analyzer is also compatible with the proposals of realistic QND detection [85,88–90] for single photons; however, as we have shown, it is more efficient than the standard ones for several reasons: Our QND detector can work in a passive way and can faithfully distinguish photon numbers subsequently passing through it in an even-odd basis. Furthermore, it is error tolerant, when it is used to detect linearly polarized photons.

Our description of scattering imperfections includes the following: finite photon-pulse bandwidth σ_ω , cavity loss κ_s , and finite coupling g . This realistic scattering process leads to a hybrid entangled state of a photon and a QD, consisting of ideal scattering component and the error scattering component. When the two QDs couple equally to their respective micropillar cavities, the error component is passively filtered out by a PBS and then is heralded by a click of a single-photon destructive detector, leading to an inconclusive result rather than an unfaithful GHZ-state analysis. In practice, the two QDs might be different due to inhomogeneous broadening and could couple differently to their respective cavities [87]. This would lead to different scattering processes, which result in

different hybrid entangled states of a photon and a QD, when a photon is reflected by different QND detectors. This effect, in principle, can be suppressed by inserting a passive modulator before the QND detector with a larger ideal scattering component and by tuning it to match that of the other QND detector [109].

Furthermore, a QD is a candidate for quantum information processing due to its very good characteristics concerning its optical initialization, single-qubit manipulation, and readout, based on well-developed semiconductor technologies [97,103,110–112]. The coherence time of a QD electron spin can be several microseconds at temperatures around 4 K [87,103], while a single-photon scattering is accomplished on nanosecond time scales. Moreover, the present protocol of entanglement analysis can be generalized to other systems with a required level structure [113,114]. Recently, a five-photon polarization-encoded cluster state has been demonstrated with a confined dark exciton in a QD [113] and an all-photonic quantum repeater protocol was described with a similar solid-state four-level emitter [114].

VII. CONCLUSIONS

In summary, we proposed a resource-efficient analyzer of Bell and Greenberger-Horne-Zeilinger states of multiphoton systems. Quantum-nondemolition detection is implemented in our analyzer with two four-level emitters (e.g., quantum dots), each coupled to a one-dimensional system (such as optical micropillar cavity or a photonic nanocrystal waveguide). This QND measures the number of photons passing through it in the even-odd basis and constitutes a faithful element for the GHZ-state analyzer by introducing a passively error-filtering structure with linear optics.

The main idea of our proposal can be simply explained in terms of stabilizers for GHZ states defined in Eq. (6). Specifically, we proposed to measure the parity of the X -type stabilizer [$k = 1$ in Eq. (6)] with two quantum dots and to measure the parity of the Z -type stabilizers [$k = 2, 3, \dots, n$ in Eq. (6)] with direct polarization measurements on each photon scattered by the QDs. There are neither active operations nor adaptive switching in the proposed method, since the faithful GHZ-state analysis for multiple photon systems works efficiently by passively arranging two QND detectors, single-photon destructive detectors, and linear-optical elements. Furthermore, the described method is universal, as it enables two-photon Bell-state and multiphoton GHZ-state analyses. All these distinct characteristics make the proposed passive analyzers simple and resource efficient for long-distance multinode quantum communication and quantum networks.

ACKNOWLEDGMENTS

This work was supported in part by the National Key R&D Program of China (Grant No. 2017YFA0303703), the Natural Science Foundation of Jiangsu Province (Grant No. BK20180461), the National Natural and Science Foundation of China (Grants No. 11874212, No. 11574145, No. 11890700, No. 11890704, No. 11904171, and No. 11690031), and the Fundamental Research Funds for the Central Universities (Grant No. 021314380095). A.M. and F.N. acknowl-

edge a grant from the John Templeton Foundation. F.N. is also supported in part by the MURI Center for Dynamic Magneto-Optics via the Air Force Office of Scientific Research (AFOSR) (Grant No. FA9550-14-1-0040), Army Research Office (ARO) (Grant No. W911NF-18-1-0358), Asian Office of Aerospace Research and Development (AOARD) (Grant No. FA2386-18-1-4045), Japan Science and Technology Agency (JST) (Q-LEAP program and CREST Grant No. JPMJCR1676), Japan Society for the Promotion of Science (JSPS) (JSPS-RFBR Grant No. 17-52-50023 and JSPS-FWO Grant No. VS.059.18N), the NYY PHI Labs, and the RIKEN-AIST Challenge Research Fund.

APPENDIX A: ANALYZER OF TWO-PHOTON POLARIZATION-ENCODED BELL STATES

Here we give a pedagogical example of our method limited to the polarization-encoded Bell-state analysis.

The passive analyzer, in principle, enables a deterministic analysis of two-photon polarization-encoded Bell states. For any two-photon system, the four Bell states can be described as follows:

$$\begin{aligned} |\phi^\pm\rangle &= \frac{1}{\sqrt{2}}(|H\rangle|H\rangle \pm |V\rangle|V\rangle), \\ |\psi^\pm\rangle &= \frac{1}{\sqrt{2}}(|H\rangle|V\rangle \pm |V\rangle|H\rangle). \end{aligned} \quad (\text{A1})$$

Photon pairs in these states, after passing through the analyzer, lead to four different results that are heralded by single-photon destructive and QND detectors.

Suppose now that the QD in each QND detector is initialized to the state $|+\rangle$. The HWP introduces a Hadamard transformation on photons passing it, i.e., $|H\rangle \rightarrow (|H\rangle + |V\rangle)/\sqrt{2}$, or $|V\rangle \rightarrow (|H\rangle - |V\rangle)/\sqrt{2}$, and evolves the states $|\phi^+\rangle$, $|\phi^-\rangle$, $|\psi^+\rangle$, and $|\psi^-\rangle$ into $|\psi_1\rangle = |\phi^+\rangle$, $|\psi_2\rangle = |\psi^+\rangle$, $|\psi_3\rangle = |\phi^-\rangle$, and $|\psi_4\rangle = -|\psi^-\rangle$, respectively. The original states $|\phi^+\rangle$ and $|\psi^+\rangle$, with a relative phase of zero, are changed into states consisting of even numbers of V -polarized photons, i.e., $|H\rangle|H\rangle$ and $|V\rangle|V\rangle$. While the original states $|\phi^-\rangle$ and $|\psi^-\rangle$ with a relative phase of π are changed into states consisting of odd numbers of V -polarized photons, i.e., $|H\rangle|V\rangle$ and $|V\rangle|H\rangle$.

Subsequently, photons in the V -polarized (H -polarized) states are reflected (transmitted) by the PBS, and are scattered by the detector QND₁ (QND₂). Photon pairs in the states $|\psi_1\rangle$, $|\psi_2\rangle$, $|\psi_3\rangle$, and $|\psi_4\rangle$, which are combined with two QDs, are changed into the states,

$$\begin{aligned} |\psi'_1\rangle &= |\phi^+\rangle|+\rangle_1|+\rangle_2, \\ |\psi'_2\rangle &= |\psi^+\rangle|-\rangle_1|-\rangle_2, \\ |\psi'_3\rangle &= -|\phi^-\rangle|+\rangle_1|+\rangle_2, \\ |\psi'_4\rangle &= |\psi^-\rangle|-\rangle_1|-\rangle_2. \end{aligned} \quad (\text{A2})$$

The original Bell states with relative phases zero and π can be distinguished from each other, according to the states of the QDs.

To read out the original polarization information of the photon pair, the HWP between two PBSs introduces a Hadamard transformation on photons passing through it and

TABLE II. Complete two-photon Bell-state analysis. Here $|ij\rangle$ represents the measurement result of the two single-photon detectors (QDs) with $|ij\rangle = \{|HH\rangle, |VV\rangle, |HV\rangle, |VH\rangle\}$ ($|ij\rangle = \{|+\rangle, |-\rangle\}$). We use the standard notation for the Bell states $|\phi^\pm\rangle$ and $|\psi^\pm\rangle$, as given in Eq. (A1).

$ HH\rangle/ VV\rangle$	$ HV\rangle/ VH\rangle$	$ ++\rangle$	$ --\rangle$
$ \phi^+\rangle$	✓		✓
$ \phi^-\rangle$	✓		✓
$ \psi^+\rangle$		✓	
$ \psi^-\rangle$		✓	✓

transforms $|\psi'_i\rangle$ into $|\psi''_i\rangle$ for $i = 1, 2, 3, 4$, with

$$\begin{aligned} |\psi''_1\rangle &= |\phi^+\rangle|+\rangle_1|+\rangle_2, \\ |\psi''_2\rangle &= |\phi^-\rangle|-\rangle_1|-\rangle_2, \\ |\psi''_3\rangle &= -|\psi^+\rangle|+\rangle_1|+\rangle_2, \\ |\psi''_4\rangle &= -|\psi^-\rangle|-\rangle_1|-\rangle_2, \end{aligned} \quad (\text{A3})$$

which transforms the photon pair state to their original state, up to an overall phase π . Therefore, we can distinguish $|\psi''_1\rangle$ and $|\psi''_2\rangle$ from $|\psi''_3\rangle$ and $|\psi''_4\rangle$ by performing single-photon destructive measurements in the vertical-horizontal basis. Thus, one can distinguish $|\phi^\pm\rangle$ from $|\psi^\pm\rangle$. Finally, we can completely identify the four Bell states by the measurement results of the single-photon destructive and QND detectors, as shown in Table II.

APPENDIX B: ANALYZER OF THREE-PHOTON POLARIZATION-ENCODED GHZ STATES

Here we give another pedagogical example of our method of state analysis for polarization-encoded three-photon GHZ states.

For a three-photon system, the eight GHZ states can be written as follows,

$$\begin{aligned} |\text{GHZ}_{00k}\rangle_{abc} &= \frac{1}{\sqrt{2}}[|H\rangle_a|H\rangle_b|H\rangle_c + (-1)^k|V\rangle_a|V\rangle_b|V\rangle_c], \\ |\text{GHZ}_{10k}\rangle_{abc} &= \frac{1}{\sqrt{2}}[|V\rangle_a|H\rangle_b|H\rangle_c + (-1)^k|H\rangle_a|V\rangle_b|V\rangle_c], \\ |\text{GHZ}_{01k}\rangle_{abc} &= \frac{1}{\sqrt{2}}[|H\rangle_a|V\rangle_b|H\rangle_c + (-1)^k|V\rangle_a|H\rangle_b|V\rangle_c], \\ |\text{GHZ}_{11k}\rangle_{abc} &= \frac{1}{\sqrt{2}}[|V\rangle_a|V\rangle_b|H\rangle_c + (-1)^k|H\rangle_a|H\rangle_b|V\rangle_c]. \end{aligned} \quad (\text{B1})$$

To distinguish these eight GHZ states from one another, we input photons (a, b, c) into the setup for the GHZ-state analysis. Photons (a, b, c) in the GHZ states $|\text{GHZ}_{ijk}\rangle_{abc}$, $i, j, k \in \{0, 1\}$ pass through the HWP that performs a Hadamard operation on them, and are changed, respectively, into the states,

$$\begin{aligned} |\Phi_{ij0}\rangle_{abc} &= \frac{1}{2}(|G_0^{ij}\rangle + \sqrt{3}|G_2^{ij}\rangle), \\ |\Phi_{ij1}\rangle_{abc} &= \frac{1}{2}(\sqrt{3}|G_1^{ij}\rangle + |G_3^{ij}\rangle), \end{aligned} \quad (\text{B2})$$

TABLE III. Complete three-photon GHZ-state analysis. Here the measurement results C1, C2, C3, and C4 of the two single-photon detectors D_1 and D_2 correspond to either $|HHH\rangle$ or $|VVV\rangle$, and similarly for $|HVV\rangle$ or $|VHH\rangle$, $|VHV\rangle$ or $|H VH\rangle$, and $|VVH\rangle$ or $|H HV\rangle$, respectively. Here, $|+-\rangle$ and $|--\rangle$ denote two possible results of the measurement on the two QDs.

	C1	C2	C3	C4	$ +-\rangle$	$ --\rangle$
$ \text{GHZ}_{000}\rangle$	✓				✓	
$ \text{GHZ}_{001}\rangle$	✓					✓
$ \text{GHZ}_{100}\rangle$		✓			✓	
$ \text{GHZ}_{101}\rangle$		✓				✓
$ \text{GHZ}_{010}\rangle$			✓		✓	
$ \text{GHZ}_{011}\rangle$			✓			✓
$ \text{GHZ}_{110}\rangle$				✓	✓	
$ \text{GHZ}_{111}\rangle$				✓		✓

where the ancillary states $|G_m^{ij}\rangle$ with $m = 0, 1, 2, 3$, are given in Sec. III C and can be detailed as follows:

$$\begin{aligned} |G_0^{ij}\rangle &= |H\rangle_a|H\rangle_b|H\rangle_c, \\ |G_1^{ij}\rangle &= \frac{\sigma_{z_a}^i \otimes \sigma_{z_b}^j}{\sqrt{3}}(|V\rangle_a|H\rangle_b|H\rangle_c \\ &\quad + |H\rangle_a|V\rangle_b|H\rangle_c + |H\rangle_a|H\rangle_b|V\rangle_c), \\ |G_2^{ij}\rangle &= \frac{\sigma_{z_a}^i \otimes \sigma_{z_b}^j}{\sqrt{3}}(|H\rangle_a|V\rangle_b|V\rangle_c \\ &\quad + |V\rangle_a|H\rangle_b|V\rangle_c + |V\rangle_a|V\rangle_b|H\rangle_c), \\ |G_3^{ij}\rangle &= \sigma_{z_a}^i \otimes \sigma_{z_b}^j|V\rangle_a|V\rangle_b|V\rangle_c. \end{aligned} \quad (\text{B3})$$

The GHZ states $|\text{GHZ}_{ijk}\rangle_{abc}$ ($|\text{GHZ}_{ij1}\rangle_{abc}$) with the relative phase 0 (π) can be distinguished from one another by measuring the numbers of V-polarized photons in the even-odd basis with QND detectors. The QND detectors initialized to the state $|+\rangle$ flip the states of the QD and photon during the scattering process, and evolve photons (a, b, c) and two QDs into the states:

$$\begin{aligned} |\Phi'_{ij0}\rangle_{abc} &= \frac{\sigma_{x_a} \otimes \sigma_{x_b} \otimes \sigma_{x_c}}{2}(|G_0^{ij}\rangle + \sqrt{3}|G_2^{ij}\rangle)|+\rangle_1|-\rangle_2, \\ |\Phi'_{ij1}\rangle_{abc} &= \frac{\sigma_{x_a} \otimes \sigma_{x_b} \otimes \sigma_{x_c}}{2}(\sqrt{3}|G_1^{ij}\rangle + |G_3^{ij}\rangle)|-\rangle_1|+\rangle_2. \end{aligned} \quad (\text{B4})$$

The original GHZ states with relative phases 0 and π can be distinguished from one another, according to the states of the QDs.

To read out the original polarization information of photons (a, b, c) , the HWP between two PBSs introduces a Hadamard transformation on photons passing through it and transforms $|\Phi'_{ijk}\rangle$ into $|\Phi''_{ijk}\rangle$ with

$$\begin{aligned} |\Phi''_{ij0}\rangle_{abc} &= (-1)^{i+j}|\text{GHZ}_{ij1}\rangle_{abc}|+\rangle_1|-\rangle_2, \\ |\Phi''_{ij1}\rangle_{abc} &= (-1)^{i+j}|\text{GHZ}_{ij0}\rangle_{abc}|-\rangle_1|+\rangle_2. \end{aligned} \quad (\text{B5})$$

Now the photons (a, b, c) are transformed to their original state, up to a phase difference π , which is independent of the results

of the single-photon destructive measurements in the vertical-horizontal basis. Therefore, we can completely identify the

eight GHZ states by the measurement results of the single-photon destructive and QND detectors, as shown in Table III.

-
- [1] R. Horodecki, P. Horodecki, M. Horodecki, and K. Horodecki, Quantum entanglement, *Rev. Mod. Phys.* **81**, 865 (2009).
 - [2] H. J. Kimble, The quantum internet, *Nature (London)* **453**, 1023 (2008).
 - [3] J. I. Cirac, A. K. Ekert, S. F. Huelga, and C. Macchiavello, Distributed quantum computation over noisy channels, *Phys. Rev. A* **59**, 4249 (1999).
 - [4] Y. L. Lim, A. Beige, and L. C. Kwek, Repeat-Until-Success Linear Optics Distributed Quantum Computing, *Phys. Rev. Lett.* **95**, 030505 (2005).
 - [5] L. Jiang, J. M. Taylor, A. S. Sørensen, and M. D. Lukin, Distributed quantum computation based on small quantum registers, *Phys. Rev. A* **76**, 062323 (2007).
 - [6] W. Qin, X. Wang, A. Miranowicz, Z. Zhong, and F. Nori, Heralded quantum controlled-phase gates with dissipative dynamics in macroscopically distant resonators, *Phys. Rev. A* **96**, 012315 (2017).
 - [7] H.-K. Lo, M. Curty, and K. Tamaki, Secure quantum key distribution, *Nat. Photon.* **8**, 595 (2014).
 - [8] C. H. Bennett, G. Brassard, C. Crépeau, R. Jozsa, A. Peres, and W. K. Wootters, Teleporting an Unknown Quantum State Via Dual Classical and Einstein-Podolsky-Rosen Channels, *Phys. Rev. Lett.* **70**, 1895 (1993).
 - [9] S. Pirandola, J. Eisert, C. Weedbrook, A. Furusawa, and S. L. Braunstein, Advances in quantum teleportation, *Nat. Photon.* **9**, 641 (2015).
 - [10] N. Gisin, G. Ribordy, W. Tittel, and H. Zbinden, Quantum cryptography, *Rev. Mod. Phys.* **74**, 145 (2002).
 - [11] W. Dür, H.-J. Briegel, J. I. Cirac, and P. Zoller, Quantum repeaters based on entanglement purification, *Phys. Rev. A* **59**, 169 (1999).
 - [12] L. Jiang, J. M. Taylor, K. Nemoto, W. J. Munro, R. Van Meter, and M. D. Lukin, Quantum repeater with encoding, *Phys. Rev. A* **79**, 032325 (2009).
 - [13] T.-J. Wang, S.-Y. Song, and G. L. Long, Quantum repeater based on spatial entanglement of photons and quantum-dot spins in optical microcavities, *Phys. Rev. A* **85**, 062311 (2012).
 - [14] W. J. Munro, A. M. Stephens, S. J. Devitt, K. A. Harrison, and K. Nemoto, Quantum communication without the necessity of quantum memories, *Nat. Photon.* **6**, 777 (2012).
 - [15] C. H. Bennett, G. Brassard, S. Popescu, B. Schumacher, J. A. Smolin, and W. K. Wootters, Purification of Noisy Entanglement and Faithful Teleportation Via Noisy Channels, *Phys. Rev. Lett.* **76**, 722 (1996).
 - [16] D. Deutsch, A. Ekert, R. Jozsa, C. Macchiavello, S. Popescu, and A. Sanpera, Quantum Privacy Amplification and the Security of Quantum Cryptography Over Noisy Channels, *Phys. Rev. Lett.* **77**, 2818 (1996).
 - [17] Y.-B. Sheng, F.-G. Deng, and H.-Y. Zhou, Efficient polarization-entanglement purification based on parametric down-conversion sources with cross-Kerr nonlinearity, *Phys. Rev. A* **77**, 042308 (2008).
 - [18] Y.-B. Sheng and F.-G. Deng, Deterministic entanglement purification and complete nonlocal Bell-state analysis with hyperentanglement, *Phys. Rev. A* **81**, 032307 (2010).
 - [19] M. Żukowski, A. Zeilinger, M. A. Horne, and A. K. Ekert, “Event-Ready-Detectors” Bell Experiment Via Entanglement Swapping, *Phys. Rev. Lett.* **71**, 4287 (1993).
 - [20] L. Chen and W. She, Hybrid entanglement swapping of photons: Creating the orbital angular momentum Bell states and Greenberger-Horne-Zeilinger states, *Phys. Rev. A* **83**, 012306 (2011).
 - [21] C. Y. Hu and J. G. Rarity, Loss-resistant state teleportation and entanglement swapping using a quantum-dot spin in an optical microcavity, *Phys. Rev. B* **83**, 115303 (2011).
 - [22] Y.-N. Chen, S.-L. Chen, N. Lambert, C.-M. Li, G.-Y. Chen, and F. Nori, Entanglement swapping and testing quantum steering into the past via collective decay, *Phys. Rev. A* **88**, 052320 (2013).
 - [23] X. Su, C. Tian, X. Deng, Q. Li, C. Xie, and K. Peng, Quantum Entanglement Swapping Between Two Multipartite Entangled States, *Phys. Rev. Lett.* **117**, 240503 (2016).
 - [24] G.-L. Long and X.-S. Liu, Theoretically efficient high-capacity quantum-key-distribution scheme, *Phys. Rev. A* **65**, 032302 (2002).
 - [25] F.-G. Deng, G. L. Long, and X.-S. Liu, Two-step quantum direct communication protocol using the Einstein-Podolsky-Rosen pair block, *Phys. Rev. A* **68**, 042317 (2003).
 - [26] J.-Y. Hu, B. Yu, M.-Y. Jing, L.-T. Xiao, S.-T. Jia, G.-Q. Qin, and G.-L. Long, Experimental quantum secure direct communication with single photons, *Light Sci. Appl.* **5**, e16144 (2016).
 - [27] W. Zhang, D.-S. Ding, Y.-B. Sheng, L. Zhou, B.-S. Shi, and G.-C. Guo, Quantum Secure Direct Communication with Quantum Memory, *Phys. Rev. Lett.* **118**, 220501 (2017).
 - [28] J.-W. Pan, Z.-B. Chen, C.-Y. Lu, H. Weinfurter, A. Zeilinger, and M. Żukowski, Multiphoton entanglement and interferometry, *Rev. Mod. Phys.* **84**, 777 (2012).
 - [29] F.-G. Deng, B.-C. Ren, and X.-H. Li, Quantum hyperentanglement and its applications in quantum information processing, *Sci. Bull.* **62**, 46 (2017).
 - [30] T. Tashima, M. S. Tame, S. K. Özdemir, F. Nori, M. Koashi, and H. Weinfurter, Photonic multipartite entanglement conversion using nonlocal operations, *Phys. Rev. A* **94**, 052309 (2016).
 - [31] M. Hillery, V. Bužek, and A. Berthiaume, Quantum secret sharing, *Phys. Rev. A* **59**, 1829 (1999).
 - [32] S. Schauer, M. Huber, and B. C. Hiesmayr, Experimentally feasible security check for n -qubit quantum secret sharing, *Phys. Rev. A* **82**, 062311 (2010).
 - [33] A. Farouk, J. Batle, M. Elhoseny, M. Naseri, M. Lone, A. Fedorov, M. Alkhambashi, S. H. Ahmed, and M. Abdel-Aty, Robust general N user authentication scheme in a centralized quantum communication network via generalized GHZ states, *Front. Phys.* **13**, 130306 (2018).
 - [34] L. Dong, Y.-F. Lin, C. Cui, H.-K. Dong, X.-M. Xiu, and Y.-J. Gao, Fault-tolerant distribution of GHZ states and controlled DSQC based on parity analyses, *Opt. Express* **25**, 18581 (2017).
 - [35] J. Ribeiro, G. Murta, and S. Wehner, Fully device-independent conference key agreement, *Phys. Rev. A* **97**, 022307 (2018).

- [36] H. J. Briegel, D. E. Browne, W. Dür, R. Raussendorf, and M. Van den Nest, Measurement-based quantum computation, *Nat. Phys.* **5**, 19 (2009).
- [37] T. Tanamoto, Y.-X. Liu, S. Fujita, X. Hu, and F. Nori, Producing Cluster States in Charge Qubits and Flux Qubits, *Phys. Rev. Lett.* **97**, 230501 (2006).
- [38] J. Q. You, X.-B. Wang, T. Tanamoto, and F. Nori, Efficient one-step generation of large cluster states with solid-state circuits, *Phys. Rev. A* **75**, 052319 (2007).
- [39] T. Tanamoto, Y.-X. Liu, X. Hu, and F. Nori, Efficient Quantum Circuits for One-Way Quantum Computing, *Phys. Rev. Lett.* **102**, 100501 (2009).
- [40] S. E. Economou, N. Lindner, and T. Rudolph, Optically Generated 2-Dimensional Photonic Cluster State from Coupled Quantum Dots, *Phys. Rev. Lett.* **105**, 093601 (2010).
- [41] M. Gimeno-Segovia, P. Shadbolt, D. E. Browne, and T. Rudolph, From Three-Photon Greenberger-Horne-Zeilinger States to Ballistic Universal Quantum Computation, *Phys. Rev. Lett.* **115**, 020502 (2015).
- [42] Y. Li, P. C. Humphreys, G. J. Mendoza, and S. C. Benjamin, Resource Costs for Fault-Tolerant Linear Optical Quantum Computing, *Phys. Rev. X* **5**, 041007 (2015).
- [43] V. Giovannetti, S. Lloyd, and L. Maccone, Quantum-enhanced measurements: beating the standard quantum limit, *Science* **306**, 1330 (2004).
- [44] W. Dür, M. Skotiniotis, F. Fröwis, and B. Kraus, Improved Quantum Metrology Using Quantum Error Correction, *Phys. Rev. Lett.* **112**, 080801 (2014).
- [45] L. F. Wei, Y.-X. Liu, and F. Nori, Generation and Control of Greenberger-Horne-Zeilinger Entanglement in Superconducting Circuits, *Phys. Rev. Lett.* **96**, 246803 (2006).
- [46] Y.-D. Wang, S. Chesi, D. Loss, and C. Bruder, One-step multiqubit Greenberger-Horne-Zeilinger state generation in a circuit QED system, *Phys. Rev. B* **81**, 104524 (2010).
- [47] V. Macrì, F. Nori, and A. F. Kockum, Simple preparation of Bell and Greenberger-Horne-Zeilinger states using ultrastrong-coupling circuit QED, *Phys. Rev. A* **98**, 062327 (2018).
- [48] T. Monz, P. Schindler, J. T. Barreiro, M. Chwalla, D. Nigg, W. A. Coish, M. Harlander, W. Hänsel, M. Hennrich, and R. Blatt, 14-Qubit Entanglement: Creation and Coherence, *Phys. Rev. Lett.* **106**, 130506 (2011).
- [49] H. Kaufmann, T. Ruster, C. T. Schmiegelow, M. A. Luda, V. Kaushal, J. Schulz, D. von Lindenfels, F. Schmidt-Kaler, and U. G. Poschinger, Scalable Creation of Long-Lived Multiparticle Entanglement, *Phys. Rev. Lett.* **119**, 150503 (2017).
- [50] C.-S. Yu, X. X. Yi, H.-S. Song, and D. Mei, Robust preparation of Greenberger-Horne-Zeilinger and W states of three distant atoms, *Phys. Rev. A* **75**, 044301 (2007).
- [51] A. Zheng, J. Li, R. Yu, X.-Y. Lü, and Y. Wu, Generation of Greenberger-Horne-Zeilinger state of distant diamond nitrogen-vacancy centers via nanocavity input-output process, *Opt. Express* **20**, 16902 (2012).
- [52] F. Reiter, D. Reeb, and A. S. Sørensen, Scalable Dissipative Preparation of Many-Body Entanglement, *Phys. Rev. Lett.* **117**, 040501 (2016).
- [53] X. Q. Shao, J. H. Wu, X. X. Yi, and G.-L. Long, Dissipative preparation of steady Greenberger-Horne-Zeilinger states for Rydberg atoms with quantum Zeno dynamics, *Phys. Rev. A* **96**, 062315 (2017).
- [54] Y.-F. Huang, B.-H. Liu, L. Peng, Y.-H. Li, L. Li, C.-F. Li, and G.-C. Guo, Experimental generation of an eight-photon Greenberger-Horne-Zeilinger state, *Nat. Commun.* **2**, 546 (2011).
- [55] X.-C. Yao, T.-X. Wang, P. Xu, H. Lu, G.-S. Pan, X.-H. Bao, C.-Z. Peng, C.-Y. Lu, Y.-A. Chen, and J.-W. Pan, Observation of eight-photon entanglement, *Nat. Photon.* **6**, 225 (2012).
- [56] M. Malik, M. Erhard, M. Huber, M. Krenn, R. Fickler, and A. Zeilinger, Multi-photon entanglement in high dimensions, *Nat. Photon.* **10**, 248 (2016).
- [57] M. Krenn, M. Malik, R. Fickler, R. Lapkiewicz, and A. Zeilinger, Automated Search for New Quantum Experiments, *Phys. Rev. Lett.* **116**, 090405 (2016).
- [58] M. Krenn, A. Hochrainer, M. Lahiri, and A. Zeilinger, Entanglement by Path Identity, *Phys. Rev. Lett.* **118**, 080401 (2017).
- [59] N. Bergamasco, M. Menotti, J. E. Sipe, and M. Liscidini, Generation of Path-Encoded Greenberger-Horne-Zeilinger States, *Phys. Rev. Applied* **8**, 054014 (2017).
- [60] E. Megidish, T. Shacham, A. Halevy, L. Dovrat, and H. S. Eisenberg, Resource Efficient Source of Multiphoton Polarization Entanglement, *Phys. Rev. Lett.* **109**, 080504 (2012).
- [61] L.-M. Duan and H. J. Kimble, Scalable Photonic Quantum Computation Through Cavity-Assisted Interactions, *Phys. Rev. Lett.* **92**, 127902 (2004).
- [62] Y. Li, L. Aolita, and L. C. Kwek, Photonic multiqubit states from a single atom, *Phys. Rev. A* **83**, 032313 (2011).
- [63] Y. Hao, G. Lin, K. Xia, X. Lin, Y. Niu, and S. Gong, Quantum controlled-phase-flip gate between a flying optical photon and a Rydberg atomic ensemble, *Sci. Rep.* **5**, 10005 (2015).
- [64] A. Reiserer, N. Kalb, G. Rempe, and S. Ritter, A quantum gate between a flying optical photon and a single trapped atom, *Nature (London)* **508**, 237 (2014).
- [65] A. Reiserer and G. Rempe, Cavity-based quantum networks with single atoms and optical photons, *Rev. Mod. Phys.* **87**, 1379 (2015).
- [66] S. Perseguers, G. Lapeyre Jr, D. Cavalcanti, M. Lewenstein, and A. Acín, Distribution of entanglement in large-scale quantum networks, *Rep. Prog. Phys.* **76**, 096001 (2013).
- [67] S. Bose, V. Vedral, and P. L. Knight, Multiparticle generalization of entanglement swapping, *Phys. Rev. A* **57**, 822 (1998).
- [68] C.-Y. Lu, T. Yang, and J.-W. Pan, Experimental Multiparticle Entanglement Swapping for Quantum Networking, *Phys. Rev. Lett.* **103**, 020501 (2009).
- [69] J.-W. Pan and A. Zeilinger, Greenberger-Horne-Zeilinger-state analyzer, *Phys. Rev. A* **57**, 2208 (1998).
- [70] P. Kok, W. J. Munro, K. Nemoto, T. C. Ralph, J. P. Dowling, and G. J. Milburn, Linear optical quantum computing with photonic qubits, *Rev. Mod. Phys.* **79**, 135 (2007).
- [71] J. Calsamiglia and N. Lütkenhaus, Maximum efficiency of a linear-optical Bell-state analyzer, *Appl. Phys. B* **72**, 67 (2001).
- [72] J. Qian, X.-L. Feng, and S.-Q. Gong, Universal Greenberger-Horne-Zeilinger-state analyzer based on two-photon polarization parity detection, *Phys. Rev. A* **72**, 052308 (2005).
- [73] Y. Xia, Y.-H. Kang, and P.-M. Lu, Complete polarized photons Bell-states and Greenberger-Horne-Zeilinger-states analysis assisted by atoms, *J. Opt. Soc. Am. B* **31**, 2077 (2014).
- [74] L. Zhou and Y.-B. Sheng, Complete logic Bell-state analysis assisted with photonic Faraday rotation, *Phys. Rev. A* **92**, 042314 (2015).

- [75] Y.-B. Sheng, F.-G. Deng, and G. L. Long, Complete hyperentangled-Bell-state analysis for quantum communication, *Phys. Rev. A* **82**, 032318 (2010).
- [76] B.-C. Ren, H.-R. Wei, M. Hua, T. Li, and F.-G. Deng, Complete hyperentangled-Bell-state analysis for photon systems assisted by quantum-dot spins in optical microcavities, *Opt. Express* **20**, 24664 (2012).
- [77] T.-J. Wang, Y. Lu, and G. L. Long, Generation and complete analysis of the hyperentangled Bell state for photons assisted by quantum-dot spins in optical microcavities, *Phys. Rev. A* **86**, 042337 (2012).
- [78] Q. Liu and M. Zhang, Generation and complete nondestructive analysis of hyperentanglement assisted by nitrogen-vacancy centers in resonators, *Phys. Rev. A* **91**, 062321 (2015).
- [79] G.-Y. Wang, Q. Ai, B.-C. Ren, T. Li, and F.-G. Deng, Error-detected generation and complete analysis of hyperentangled Bell states for photons assisted by quantum-dot spins in double-sided optical microcavities, *Opt. Express* **24**, 28444 (2016).
- [80] D. Witthaut, M. D. Lukin, and A. S. Sørensen, Photon sorters and QND detectors using single photon emitters, *Europhys. Lett.* **97**, 50007 (2012).
- [81] J. P. Reithmaier, G. Sek, A. Löffler, C. Hofmann, S. Kuhn, S. Reitzenstein, L. Keldysh, V. Kulakovskii, T. Reinecke, and A. Forchel, Strong coupling in a single quantum dot–semiconductor microcavity system, *Nature (London)* **432**, 197 (2004).
- [82] M. Arcari, I. Söllner, A. Javadi, S. Lindskov Hansen, S. Mahmoodian, J. Liu, H. Thyrrstrup, E. H. Lee, J. D. Song, S. Stobbe, and P. Lodahl, Near-Unity Coupling Efficiency of a Quantum Emitter to a Photonic Crystal Waveguide, *Phys. Rev. Lett.* **113**, 093603 (2014).
- [83] T. Li, A. Miranowicz, X. Hu, K. Xia, and F. Nori, Quantum memory and gates using a Λ -type quantum emitter coupled to a chiral waveguide, *Phys. Rev. A* **97**, 062318 (2018).
- [84] P. Lodahl, S. Mahmoodian, and S. Stobbe, Interfacing single photons and single quantum dots with photonic nanostructures, *Rev. Mod. Phys.* **87**, 347 (2015).
- [85] C. Y. Hu, A. Young, J. L. O’Brien, W. J. Munro, and J. G. Rarity, Giant optical Faraday rotation induced by a single-electron spin in a quantum dot: applications to entangling remote spins via a single photon, *Phys. Rev. B* **78**, 085307 (2008).
- [86] C. Y. Hu, W. J. Munro, and J. G. Rarity, Deterministic photon entangler using a charged quantum dot inside a microcavity, *Phys. Rev. B* **78**, 125318 (2008).
- [87] R. J. Warburton, Single spins in self-assembled quantum dots, *Nat. Mater.* **12**, 483 (2013).
- [88] C. O’Brien, T. Zhong, A. Faraon, and C. Simon, Nondestructive photon detection using a single rare-earth ion coupled to a photonic cavity, *Phys. Rev. A* **94**, 043807 (2016).
- [89] D. Witthaut and A. S. Sørensen, Photon scattering by a three-level emitter in a one-dimensional waveguide, *New J. Phys.* **12**, 043052 (2010).
- [90] A. Reiserer, S. Ritter, and G. Rempe, Nondestructive detection of an optical photon, *Science* **342**, 1349 (2013).
- [91] Y. Li, L. Aolita, D. E. Chang, and L. C. Kwek, Robust-Fidelity Atom-Photon Entangling Gates in the Weak-Coupling Regime, *Phys. Rev. Lett.* **109**, 160504 (2012).
- [92] T. Li and F.-G. Deng, Error-rejecting quantum computing with solid-state spins assisted by low- Q optical microcavities, *Phys. Rev. A* **94**, 062310 (2016).
- [93] D. Gottesman, Class of quantum error-correcting codes saturating the quantum hamming bound, *Phys. Rev. A* **54**, 1862 (1996).
- [94] G. Tóth and O. Gühne, Entanglement detection in the stabilizer formalism, *Phys. Rev. A* **72**, 022340 (2005).
- [95] C. Schmid, N. Kiesel, W. Laskowski, W. Wieczorek, M. Żukowski, and H. Weinfurter, Discriminating Multipartite Entangled States, *Phys. Rev. Lett.* **100**, 200407 (2008).
- [96] C. Greganti, M.-C. Roehsner, S. Barz, M. Waegell, and P. Walther, Practical and efficient experimental characterization of multiqubit stabilizer states, *Phys. Rev. A* **91**, 022325 (2015).
- [97] I. Buluta, S. Ashhab, and F. Nori, Natural and artificial atoms for quantum computation, *Rep. Prog. Phys.* **74**, 104401 (2011).
- [98] V. Giesz, N. Somaschi, G. Hornecker, T. Grange, B. Reznychenko, L. De Santis, J. Demory, C. Gomez, I. Sagnes, A. Lemaître *et al.*, Coherent manipulation of a solid-state artificial atom with few photons, *Nat. Commun.* **7**, 11986 (2016).
- [99] N. Somaschi, V. Giesz, L. De Santis, J. Loredo, M. P. Almeida, G. Hornecker, S. L. Portalupi, T. Grange, C. Antón, J. Demory, C. Gómez, I. Sagnes, N. D. Lanzillotti-Kimura, A. Lemaître, A. Auffeves, A. G. White, L. Lanço, and P. Senellart, Near-optimal single-photon sources in the solid state, *Nat. Photon.* **10**, 340 (2016).
- [100] D. P. DiVincenzo and F. Solgun, Multi-qubit parity measurement in circuit quantum electrodynamics, *New J. Phys.* **15**, 075001 (2013).
- [101] I. Cohen and K. Mølmer, Deterministic quantum network for distributed entanglement and quantum computation, *Phys. Rev. A* **98**, 030302(R) (2018).
- [102] M. H. Mikkelsen, J. Berezovsky, N. G. Stoltz, L. A. Coldren, and D. D. Awschalom, Optically detected coherent spin dynamics of a single electron in a quantum dot, *Nat. Phys.* **3**, 770 (2007).
- [103] K. De Greve, D. Press, P. L. McMahon, and Y. Yamamoto, Ultrafast optical control of individual quantum dot spin qubits, *Rep. Prog. Phys.* **76**, 092501 (2013).
- [104] X.-L. Wang, L.-K. Chen, W. Li, H.-L. Huang, C. Liu, C. Chen, Y.-H. Luo, Z.-E. Su, D. Wu, Z.-D. Li, H. Lu, Y. Hu, X. Jiang, C.-Z. Peng, L. Li, N.-L. Liu, Y.-A. Chen, C.-Y. Lu, and J.-W. Pan, Experimental Ten-Photon Entanglement, *Phys. Rev. Lett.* **117**, 210502 (2016).
- [105] L.-K. Chen, Z.-D. Li, X.-C. Yao, M. Huang, W. Li, H. Lu, X. Yuan, Y.-B. Zhang, X. Jiang, C.-Z. Peng, L. Li, N.-L. Liu, X. Ma, C.-Y. Lu, Y.-A. Chen, and J.-W. Pan, Observation of ten-photon entanglement using thin BiB_3O_6 crystals, *Optica* **4**, 77 (2017).
- [106] T. B. Pittman, B. C. Jacobs, and J. D. Franson, Demonstration of Nondeterministic Quantum Logic Operations Using Linear Optical Elements, *Phys. Rev. Lett.* **88**, 257902 (2002).
- [107] Y. Hasegawa, R. Ikuta, N. Matsuda, K. Tamaki, H.-K. Lo, T. Yamamoto, K. Azuma, and N. Imoto, Experimental time-reversed adaptive Bell measurement towards all-photonic quantum repeaters, *Nat. Commun.* **10**, 378 (2019).
- [108] Z.-D. Li, R. Zhang, X.-F. Yin, L.-Z. Liu, Y. Hu, Y.-Q. Fang, Y.-Y. Fei, X. Jiang, J. Zhang, L. Li, N.-L. Liu, F. Xu, Y.-A.

- Chen, and J.-W. Pan, Experimental quantum repeater without quantum memory, *Nat. Photon.* **13**, 644 (2019).
- [109] T. Li, G.-J. Yang, and F.-G. Deng, Entanglement distillation for quantum communication network with atomic-ensemble memories, *Opt. Express* **22**, 23897 (2014).
- [110] R.-B. Liu, W. Yao, and L. Sham, Quantum computing by optical control of electron spins, *Adv. Phys.* **59**, 703 (2010).
- [111] P. Lodahl, Quantum-dot based photonic quantum networks, *Quantum Sci. Technol.* **3**, 013001 (2017).
- [112] X. Ding, Y. He, Z.-C. Duan, N. Gregersen, M.-C. Chen, S. Unsleber, S. Maier, C. Schneider, M. Kamp, S. Höfling, C.-Y. Lu, and J.-W. Pan, On-Demand Single Photons with High Extraction Efficiency and Near-Unity Indistinguishability from a Resonantly Driven Quantum Dot in a Micropillar, *Phys. Rev. Lett.* **116**, 020401 (2016).
- [113] I. Schwartz, D. Cogan, E. R. Schmidgall, Y. Don, L. Gantz, O. Kenneth, N. H. Lindner, and D. Gershoni, Deterministic generation of a cluster state of entangled photons, *Science* **354**, 434 (2016).
- [114] D. Buterakos, E. Barnes, and S. E. Economou, Deterministic Generation of All-Photonic Quantum Repeaters from Solid-State Emitters, *Phys. Rev. X* **7**, 041023 (2017).